Biophysical Chemistry 19 (1984) 131–145
Elsevier

BPC 00835

TRANSIENT KINETICS OF THERMODYNAMIC BUFFERING

Jörg W. STUCKI, Lilly H. LEHMANN and Peter MANI

Pharmakologisches Institut der Universität Bern, Bern, Switzerland

Received 17th October 1983
Accepted 21st November 1983

Key words: Thermodynamic buffer; Transient kinetics; Relaxation curve; Lyapunov exponents; Adenylic energy charge; Constant of motion

The transient response of mitochondrial ATP production towards perturbations was studied by analyzing the trajectories leading from arbitrary initial conditions of the adenine nucleotide pool to the final steady state. These trajectories were calculated from differential equations based on linear relations between flows and thermodynamic forces of the adenylate kinase system including oxidative phosphorylation. The motion of the system along the trajectories consists of two phases: (1) a rapid phase leading from initial states to a common relaxation curve; and (2) a slow phase leading along the relaxation curve to the final steady state. The first phase corresponds to a motion close to the loci of constant adenylic energy charge. In line with this observation is the finding that the energy charge is a constant of motion of the adenylate kinase reaction. The second phase corresponds to a motion along a relaxation curve characterized by minimal Lyapunov exponents in the concentration space of the adenine nucleotides. Thus, both phases of the transient kinetics can be approximated in terms of thermodynamic functions to a high degree of precision. Incubations with isolated rat liver mitochondria were in excellent agreement with the theoretical predictions. In summary, these studies show that the adenylate kinase system not only optimizes the efficiency of oxidative phosphorylation through thermodynamic buffering but, in addition, also deeply influences the transient response of the whole system.

1. Introduction

The most important process for the production of ATP in aerobic tissue is oxidative phosphorylation. In this process, which is localized within mitochondria, the oxidation of reducing equivalents in the form of NADH and $FADH_2$ is linked to the phosphorylation of ADP to ATP. In previous work we demonstrated that oxidative phosphorylation can be treated phenomenologically as a linear energy converter, in which the flows at input (oxygen consumption) and at output (ATP production) are linearly related to the forces at input (redox potential of the oxidizable substrates) and at output (phosphate potential) [1,2]. Furthermore, it was shown that there exists a precise value of the phosphate potential X_p where oxidative phosphorylation operates at optimal efficiency. This value was found to depend only on the degree of coupling and on the phenomenological stoichiometry of oxidative phosphorylation, for any given redox potential applied at the input of this energy converter. In particular, it was found that the system can operate at optimal efficiency if and only if the load conductance attached to oxidative phosphorylation, i.e., the irreversible ATP-utilizing reactions, is matched to the output conductance of phosphorylation. Under these conditions the optimal phosphate potential turned out to be the natural steady-state output potential of oxidative phosphorylation [1,2]. In vivo, however, this condition of conductance matching will hardly ever be fulfilled because of the natural fluctuations of the load about a matched temporal mean value.

In subsequent work [2,3] we described how a reversible ATP-utilizing reaction, the adenylate kinase reaction, can act as a thermodynamic buffer being able to maintain the phosphate potential

close to the optimal value in the presence of a fluctuating load. It was also shown that thermodynamic buffering is typically a transient phenomenon which operates only as long as the driving force for the adenylate kinase reaction, the adenylate kinase potential $X_A = -[\Delta G_A^0 + RT \ln([ATP][AMP]/[ADP]^2)]$, does not vanish. As soon as this partial reaction reaches a thermodynamic equilibrium, i.e., $X_A = 0$, the overall system is in a true steady state and thermodynamic buffering can no longer occur [3].

It was therefore of interest to study the transient kinetic behavior of the adenylate kinase system in more detail. In this paper we attempted to establish a link between a conventional kinetic description of the transients and a description within the framework of nonequilibrium thermodynamics. As is well known, the realm of nonequilibrium thermodynamics is a steady-state situation [4,5] and little can be said about transient phenomena [6]. By introducing physical concepts like constants of motion and Lyapunov exponents into the thermodynamic description we succeeded, however, in describing transient kinetic phenomena to a considerable level of sophistication on a thermodynamic basis. The aim of this paper is to illustrate how these ideas work out in the case of the adenylate kinase system. Another advantage of such a treatment will be that a new and relevant biological quantity, the degree of thermodynamic buffering of the adenylate kinase system, can then also be formulated in a consistent manner on the basis of a nonequilibrium thermodynamic description. This subject will be treated in a subsequent paper.

In this paper we first introduce a convenient state space representation of the adenylate kinase system in the form of a reaction simplex in section 2. This representation will allow an easy and intuitive understanding of special trajectories of the system such as the loci of constant adenylic energy charge, constant phosphate potential and constant adenylate kinase potential. In section 3 we describe some main features of the transient behavior of the adenylate kinase system as obtained by numerical integration of the differential equations describing the kinetics of this system. These theoretical predictions will be verified experimentally by incubations with isolated rat liver mitochondria as described in section 4. Section 5 will show how the main characteristics of the transients can be understood on the basis of a constant of motion of the adenylate kinase reaction, i.e., the adenylic

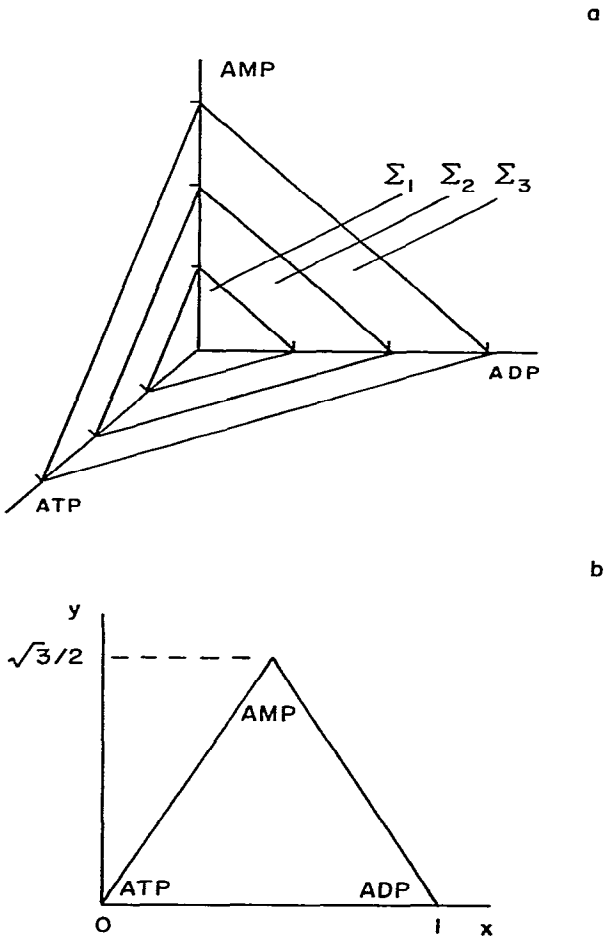

Fig. 1. The adenylate kinase reaction simplex. The upper panel (a) of this figure depicts three surfaces of constant adenine nucleotide concentrations $\Sigma_i = [ATP] + [ADP] + [AMP]$, ($i = 1, 2, 3$) in the positive orthant of the concentration space of the adenine nucleotides. Each one of these simplices may be normalized and transformed into the image space $[x, y]$ by using eqs. 1 and 2. The resulting reaction simplex which has the form of an equilateral triangle is shown in the lower part (b) of the figure.

energy charge [7], and of the relaxation curves of the system, calculated from the minimal Lyapunov exponents [8,9] of entropy production. Finally, section 6 discusses possible generalizations and applications of these concepts.

2. The adenylate kinase reaction simplex

The adenylate kinase reaction

$$ATP + AMP \rightleftharpoons 2ADP$$

involves the chemical species ATP, ADP and AMP. Hence the state of the system at any time can be described by a concentration vector $\boldsymbol{a} = ([ATP], [ADP], [AMP])^T$ in R_3^+, the positive orthant of a three-dimensional real vector space [9]. Since for the time intervals of interest for our purposes the sum of the adenine nucleotides $\Sigma = [ATP] + [ADP] + [AMP]$ can be assumed as constant, any state of the system must lie in the intersection of R_3^+ with the surface $\Sigma = \text{constant}$. Hence, our state space of interest is a two-dimensional equilateral triangle in R_3^+ which is called a reaction simplex [10]. Recently, Clarke [11] has proposed that such a state space be called a concentration polyhedron. But, since in our case we are dealing with a regular simplex [12], we prefer to stick to the conventional terminology. Fig. 1a illustrates such reaction simplices for different values of Σ.

A convenient transformation of this simplex consists of two rotations about the intersection with the [ATP] axis such that one looks perpendicularly onto the equilateral triangle in a two-dimensional image space $\{x, y\}$. This mapping $\{[ATP], [ADP], [AMP]\} \rightarrow \{x, y\}$ is given by the transformation

$$x = \frac{[ADP] + 1/2[AMP]}{\Sigma} \tag{1}$$

$$y = \frac{[AMP]\sqrt{3}}{2\Sigma} \tag{2}$$

where x and y are the projections of the rotated simplex along the abscissa and ordinate of the image plane, respectively, as shown in fig. 1b. Note that x and y are normalized by dividing through Σ in eqs. 1. and 2.

Any steady state of the system can now be represented by a point on this equilateral triangle which we call therefore the adenylate kinase reac-

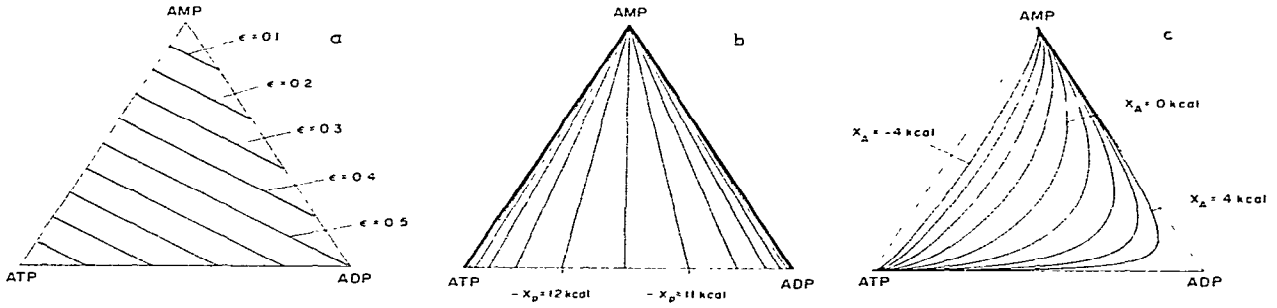

Fig. 2. Some distinguished loci in the reaction simplex. (a) The loci of constant adenylic energy charge $\varepsilon = ([ATP] + 1/2[ADP])/\Sigma$ intersect the line ATP–AMP perpendicularly. The increment of the energy charge between adjacent lines in this figure is 0.1. (b) Loci of constant phosphate potentials $X_p = -[\Delta G_p^0 + RT \ln([ATP]/[ADP]\cdot[P_i])]$ were calculated for a P_i concentration of 8 mM. The increment between adjacent loci in this figure is 0.5 kcal. The lines for $X_p < -15$ or $X_p > -8$ kcal were indistinguishable. A value of $\Delta G_p^0 = 8.5$ kcal was used throughout this study [1]. Note that the loci of constant X_p simultaneously correspond to the lines of constant [ATP]/[ADP] ratios as already pointed out by Atkinson [7]. (c) The loci of constant adenylate kinase potentials $X_A = -[\Delta G_A^0 + RT \ln([ATP]\cdot[AMP]/[ADP]^2)]$ were calculated in increments of 1 kcal. The curve labelled $X_A = 0$ corresponds to the loci along which the adenylate kinase reaction is in thermodynamic equilibrium (see also ref. 7). Note that thermodynamic buffering occurs within the region $X_A > 0$ (positive net AMP flow) whereas the regeneration of this buffer takes place in the region $X_A < 0$ (negative AMP flow). Therefore, oxidative phosphorylation is in a true steady state characterized by constant concentrations of the adenine nucleotides only along the line $X_A = 0$. Everywhere else the system is in a transient state (cf. also fig. 5). A value of $\Delta G_A^0 = 0.15$ was used throughout this study [3].

tion simplex. Such a representation has already been used by Garland [13] and Atkinson [7]. Any transition from one state of the adenylate kinase system to another can be represented by a succession of points within this simplex. The line joining these points is called a trajectory and tells which states are accessible to the system during a transition from one state to another. Note that a trajectory is an integral curve in the concentration space of the adenine nucleotides and therefore does not contain time information in an explicit manner. The temporal evolution of the system can, however, be made visible by a representation of points of the trajectory sampled at constant time intervals.

As already pointed out by Atkinson [7], there are several lines in this simplex which are of a special interest to adenine nucleotide metabolism. Fig. 2 depicts the loci of constant adenylic energy charge $\varepsilon = ([ATP] + 1/2\ [ADP])/\Sigma$ (a), of constant phosphate potentials $X_p = -[\Delta G^0_{phos} + RT \ln([ATP]/[ADP]\cdot[P_i])]$ (b) and of constant adenylate kinase potentials X_A (c). These loci will be of particular interest when analyzing the trajectories of the transients of the adenylate kinase system described in the following section.

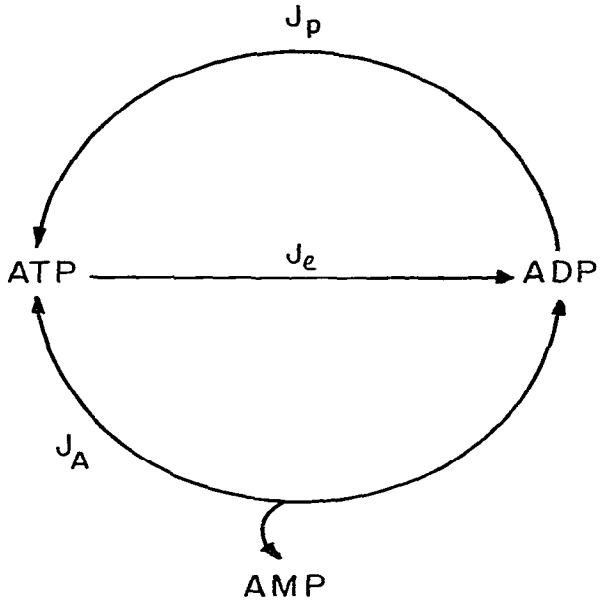

Fig. 3. Reaction scheme of oxidative phosphorylation with load and adenylate kinase. This scheme shows how the net flows J_p (phosphorylation), J_l (load) and J_A (adenylate kinase reaction) affect the adenine nucleotide concentrations. This scheme serves as the basis for the sign conventions used to formulate the differential equations (eqs. 6–8) for the adenine nucleotide concentrations.

3. Computer simulations of trajectories

In this section we will investigate how the system oxidative phosphorylation plus the adenylate kinase reaction reaches a steady state. For this purpose we study two different starting situations:

(1) Different compositions of the initial non-steady-state adenine nucleotide pool. From these initial conditions we calculate the trajectories leading to a steady state.

(2) Starting from a steady-state situation with a matched load conductance we perturb the load conductance and calculate the trajectory leading to a new steady state. When the system has reached this state we switch the load conductance back to the old matched value and observe by which path the system returns to the initial steady state.

Fig. 3 depicts how the flow components of the system affect the adenine nucleotide concentrations. There are three different net flows which we have to consider: The phosphorylation flow J_p, the load flow J_l and the adenylate kinase flow J_A. As previously shown, these flows can be expressed in terms of thermodynamic forces [1,3]:

$$J_p = L_p X_p + L_{po} X_o \tag{3}$$

$$J_l = L_l X_p \tag{4}$$

$$J_A = L_A X_A \tag{5}$$

where the L terms are the phenomenological coefficients of the system [1,3] and the X terms the thermodynamic forces. The meaning of X_A and X_p has been defined in the foregoing. X_o is the redox potential of the substrate applied to the respiratory chain [1]. As in previous work we have assumed linear relations between flows and forces in this system. The comparison between the theoretical results in this section and the actual experimental measurements in the next section will re-

veal that this assumption is perfectly legitimate. From the scheme in fig. 3 and eqs. 3–5 we can now read off the rate laws for the adenine nucleotide concentrations:

$$[\dot{A}TP] = J_p + J_l + J_A = (L_p + L_l)X_p + L_A X_A + L_{po} X_o \quad (6)$$

$$[\dot{A}DP] = -J_p - J_l - 2J_A = -(L_p + L_l)X_p - 2L_A X_A - L_{po} X_o \quad (7)$$

$$[\dot{A}MP] = J_A = L_A X_A \quad (8)$$

Inserting the definitions of the thermodynamic forces X_p and X_A yields the differential equations in terms of adenine nucleotide concentrations:

$$[\dot{A}TP] = -(L_p + L_l)\left[\Delta G_p^0 + RT \ln \frac{[ATP]}{[ADP][P_i]}\right] - L_A\left[\Delta G_A^0 + RT \ln \frac{[ATP][AMP]}{[ADP]^2}\right] + L_{po} X_o \quad (9)$$

$$[\dot{A}TP] = (L_p + L_l)\left[\Delta G_p^0 + RT \ln \frac{[ATP]}{[ADP][P_i]}\right] + 2L_A\left[\Delta G_A^0 + RT \ln \frac{[ATP][AMP]}{[ADP]^2}\right] - L_{po} X_o \quad (10)$$

$$[\dot{A}MP] = -L_A\left[\Delta G_A^0 + RT \ln \frac{[ATP][AMP]}{[ADP]^2}\right] \quad (11)$$

Note that due to the conservation condition $\Sigma =$ constant we have $[\dot{A}TP] + [\dot{A}DP] + [\dot{A}MP] = 0$. Hence one of the above equations is redundant.

In principle these differential equations could now be solved with a digital computer by using a standard method for numerical integration. The form of eqs. 9–11 has, however, one major disadvantage for numerical integration. Whenever the concentration of any adenine nucleotide becomes very small, the differentials assume large values. Thus, in a stepwise integration at a constant step size the danger of large numerical errors arises. This could even lead to negative concentrations, obvious chemical nonsense to which even the computer fiercely protests when attempting to take the logarithm of a negative number in the next integration step.

A convenient transformation to overcome this problem consists of switching to logarithmic variables:

$$\rho_T \triangleq \ln[ATP] \quad (12)$$

$$\rho_D \triangleq \ln[ADP] \quad (13)$$

$$\rho_M \triangleq \ln[AMP] \quad (14)$$

With these transformations eqs. 9–11 can be cast

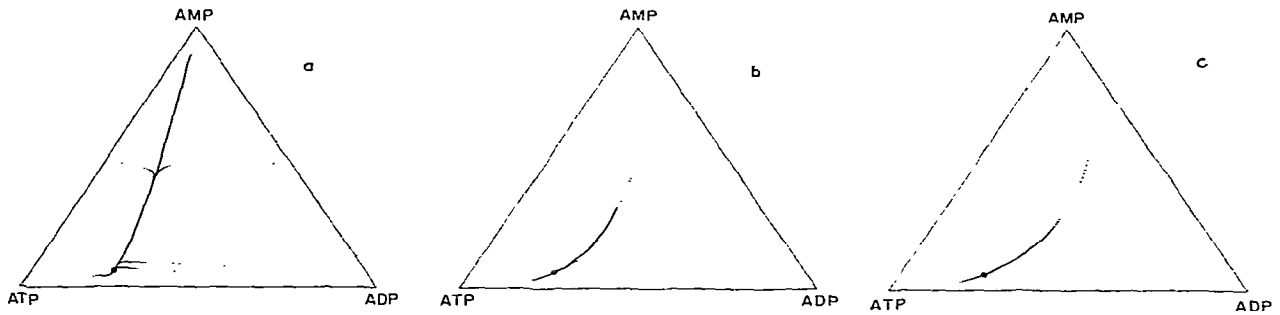

Fig. 4. Trajectories of the transients in the reaction simplex. Trajectories for the evolution of the system from different initial adenine nucleotide concentrations to the final steady state were calculated by numerical integration of eqs. 15–17 as described in the text. The parameter L_A was varied in panels a–c, namely: (a) $L_A = 0.02$, (b) $L_A = 0.2$, (c) $L_A = 1.0$. The other parameters were fixed as follows: $L_p = 0.247$, $L_{po} = 0.0785$, $L_l = 0.0749$, $X_o = 50$ kcal and $[P_i] = 8$ mM (see also ref. 2). The initial concentrations of the adenine nucleotides were chosen as shown in the figures. The final steady state is marked by an open circle. The integrated values of the adenine nucleotide concentrations were sampled at identical intervals of 0.1 arbitrary time units, transformed according to eqs. 1 and 2 and plotted in the reaction simplex. Therefore, the temporal evolution of the system becomes apparent in the trajectories. Large distances between the sampled points mean rapid evolution whereas points along a trajectory lying close together indicate a slow temporal evolution of the system. Thus, panel c with the highest value of L_A shows clearly the time scale separation of the dynamics of the system in a rapid and a slow phase of the trajectories. In contrast, panel a with a low activity of the adenylate kinase shows a rather sluggish evolution of the system into the final steady state.

into the final form used for the numerical integrations:

$$\dot{\rho}_T e^{\rho_T} = -(L_p + L_I)\left[\Delta G_p^0 + RT(\rho_T - \rho_D - \ln[P_i])\right] - L_A\left[\Delta G_A^0 + RT(\rho_T + \rho_M - 2\rho_D)\right] + L_{po}X_o \quad (15)$$

$$\dot{\rho}_D e^{\rho_D} = (L_p + L_I)\left[\Delta G_p^0 + RT(\rho_T - \rho_D - \ln[P_i])\right] - L_{po}X_o + 2L_A\left[\Delta G_A^0 + RT(\rho_T + \rho_M - 2\rho_D)\right] \quad (16)$$

$$\dot{\rho}_M e^{\rho_M} = -L_A\left[\Delta G_A^0 + RT(\rho_T + \rho_M - 2\rho_D)\right] \quad (17)$$

Note that again one of the equations is redundant due to the conservation condition:

$$\dot{\rho}_T e^{\rho_T} + \dot{\rho}_D e^{\rho_D} + \dot{\rho}_M e^{\rho_M} = 0 \quad (18)$$

In the following, eqs. 15–17 were numerically integrated with a standard fourth-order Runge-Kutta method with automatic step size control.

In a first set of simulations we have chosen different initial compositions of the adenine nucleotide pool and have calculated the trajectories leading to a steady state.

Fig. 4 depicts these trajectories for three different values of the conductance of adenylate kinase L_A. All other parameters were kept constant throughout the simulations.

The common feature of these trajectories is that they are biphasic. In a first phase the system evolves rapidly onto a line which seems to connect all the trajectories from the different starting points. In a second phase, the system then evolves slowly along this curve into the final steady state. In section 5 it will be demonstrated that this line is a relaxation curve of the system.

Another interesting finding was that the rapid phase approached a movement along a constant adenylic energy charge at high adenylate kinase activities, i.e., at high values of the conductance L_A. This becomes evident when comparing the curves in fig. 4 with fig. 2a. In section 5 we will show that the adenylic energy charge is a constant of motion of the adenylate kinase reaction. Hence, the system should indeed move along this trajectory when J_A dominates the other flows.

In summary we can state that the evolution of the system from any initial non-steady-state adenine nucleotide composition to the final steady state is biphasic: initially, a rapid movement along individual trajectories onto a relaxation curve and then a slow movement along this curve to the common attractor, the steady state.

In a second set of simulations we started the system at the steady state corresponding to a matched load conductance. Then we switched this load conductance to a mismatched value given by

$$L_I = \theta(L_I)_m \quad (19)$$

where L_I is the actual and $(L_I)_m$ the matched value of the load conductance. Hence, $0 < \theta < \infty$ is a dimensionless parameter measuring deviations from matching. When $\theta = 1$ then L_I is matched; for other θ values L_I is not matched.

The simulations were initiated by setting $\theta > 1$ as indicated in fig. 5. When the new steady state was reached, i.e., when $X_A = 0$, then θ was again set equal to 1 and the simulations were continued until $X_A = 0$ at the starting point of the simulations. Fig. 5 depicts the trajectories obtained in this fashion for three different values of L_A. All parameters, except L_I and L_A, were kept constant in this set of simulations.

It can be observed that the trajectories form a cycle when passing from the original steady state to a new steady state and back again. The trajectories corresponding to the second part of the cycle, i.e., the return to the original steady state, follow the same pattern as found in the previous simulations in fig. 4. This is not surprising, since this situation corresponds precisely to an evolution of the system from a nonstationary initial adenine nucleotide composition originating from the loci $X_A = 0$, to the steady state for $\theta = 1$.

The trajectories of the first part of the cycle, i.e., the evolution of the system from the original steady state to a new steady state upon setting $\theta > 1$ is also biphasic albeit much less clearly visible than in Fig. 4. The final part of these trajectories will again be shown to evolve along a relaxation curve in section 5. Note that the whole cycles come close to the equilibrium line $X_A = 0$ (see fig. 2c) when L_A assumes high values.

In summary it can again be said that both parts of the cycle obey biphasic kinetics characterized by a rapid initial evolution along individual trajectories and an ensuing slow movement along a relaxation curve to the steady states located on the equilibrium line of the adenylate kinase reaction.

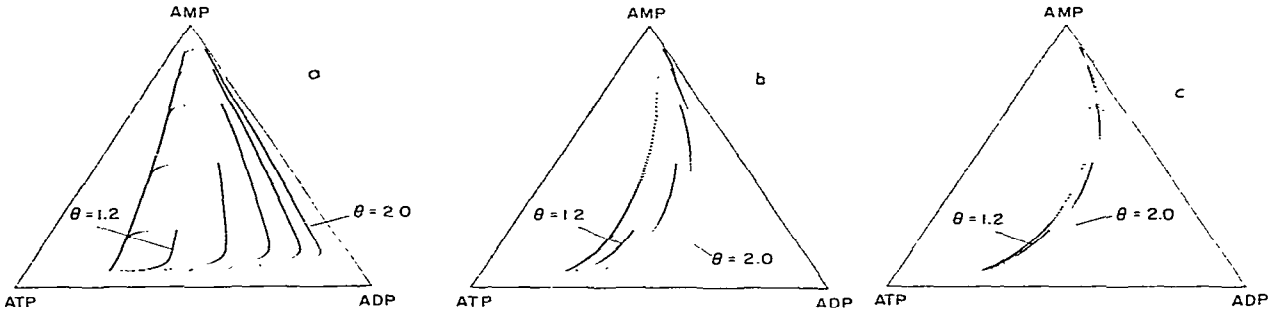

Fig. 5. Trajectories of load cycles in the reaction simplex. Panels a–c depict the trajectories of load cycles of the system for different values of the parameter L_A: (a) $L_A = 0.02$, (b) $L_A = 0.2$, (c) $L_A = 1.0$. The other parameters were again fixed to $L_p = 0.247$, $L_{po} = 0.0785$, $X_o = 50$ kcal and $[P_i] = 8$ mM. The simulations were started at the steady state corresponding to a matched load, i.e., $L_1 = \theta L_p \sqrt{1 - q^2}$ [3] with $\theta = 1$ or $L_1 = 0.0749$ with $q = q_f^{cc} = 0.953$ as used in these simulations. The values of the adenine nucleotide concentrations at the steady states were calculated with the steady state eqs. 16–21 of ref. 3. The parameter θ was then switched to the values $\theta = 1.2$, 1.4, 1.6, 1.8 and 2.0 as shown in the figures. The numerical integrations were continued until the new steady state for the mismatched load was attained, i.e., until the system reached the equilibrium line $X_A = 0$. Then θ was switched back to $\theta = 1$ and the calculation of the trajectory was continued until the system had again reached the original steady state. As in the previous figure the values of the adenine nucleotides were sampled at 0.1 time unit intervals. Again we observe a rapid and a slow phase of evolution of the trajectories into a steady state. Note that during the ascending part of the load cycles corresponding to $\theta > 1$ we have thermodynamic buffering whereas in the descending part with $\theta = 1$ the thermodynamic buffer is recharged. Panel b will again be used in fig. 8 for a direct comparison of trajectories with relaxation curves.

4. Experimental verification of trajectories

The aim of this section is to compare the theoretical predictions concerning the characteristic features of the trajectories obtained through computer simulations with experimental results. For this purpose we incubated isolated rat liver mitochondria subject to the following types of conditions:

(1) Incubations starting at different initial non-steady-state compositions of the adenine nucleotide pool. In these incubations the trajectories leading to the final steady state were measured.

(2) Incubations starting from a static head (state 4) situation. After addition of different ATP-utilizing loads in the form of ATPase we measured the trajectories leading to the final steady states of the system.

In both cases experimentally determined trajectories were compared with numerical simulations based on eqs. 15–17.

4.1. Materials and methods

Liver mitochondria from male Sprague-Dawley rats (Tierzucht Institut, Zürich, Switzerland) were isolated according to Johnson and Lardy [14] with the exception that the homogenizing medium contained 0.25 M mannitol and 0.07 M sucrose [15]. Washed mitochondria were suspended in this medium at a concentration of 1 g original liver weight per ml. ATPase used was prepared from beef heart mitochondria according to Beechy and co-workers [16].

Mitochondria were incubated at 37°C in open beakers in a water bath shaking at 100 strokes per min. The incubation medium contained 100 mM KCl, 8 mM potassium phosphate buffer (pH 7.4), 5 mM potassium glutamate (pH 7.4), 5 mM potassium malate (pH 7.4) and 1 mM $MgCl_2$. Adenine nucleotides were added at a total concentration of 2 mM. The final incubation volume was 20 ml.

In general, mitochondria were preincubated during 5 min. After the additions indicated in figs.

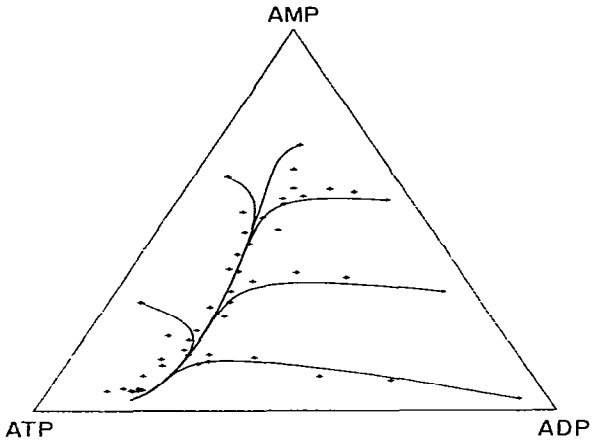

Fig. 6. Experimental verification of trajectories from different initial conditions. (+) Adenine nucleotide concentrations measured in samples taken during the incubation of isolated rat liver mitochondria as described in the text. The solid lines represent the theoretical trajectories obtained by numerical integrations of the differential equations (eqs. 15–17). The parameters for these integrations were taken from table 1 which contains the values estimated by the best fit through the experimental points with the routine MODFIT (see text). The following mean values were used and converted with eqs. 20–23 for this plot: $Z = 3.14$, $q = 0.929$, $\theta = 0.119$ and $\Pi = 2.92$. The other parameters were $X_{0} = 45$ kcal [1], $[P_i] = 8$ mM and $L_{0} = 0.027$. The initial conditions were chosen according to the experimentally determined initial concentrations of the adenine nucleotides as listed in table 1.

6 and 7 the incubations were continued by taking 1-ml samples at defined incubation periods. The samples were immediately deproteinized by addition of perchloric acid to a final concentration of 0.15 M. The deproteinized and neutralized extracts were assayed for ATP, ADP and AMP by standard enzymatic methods [17,18]. Enzymes and coenzymes were obtained from Boehringer (Mannheim, F.R.G.).

4.2. Experimental results and discussion

The results of incubations with different initial adenine nucleotide concentrations are summarized in fig. 6. In this respresentation the pooled data of six mitochondrial incubations are plotted. After addition of 2 mM adenine nucleotides of the compositions indicated in table 1, samples were taken at the following running times of the incubation: 0, 10, 15, 20, 30, 40, 60, 80, 120, 180, 240 and 300 s. Superimposed on the experimentally determined points are the trajectories obtained by numerical integration of eqs. 15–17. The initial conditions of the adenine nucleotides were chosen according to the initial composition of the adenine nucleotide pool used in the incubations. The actual P_i concentration was calculated from the initial P_i concentration and the measured adenine nucleotide concentrations taking into account the liberation

Table 1

Parameter estimations for experiments with different initial adenine nucleotide concentrations

The parameters Z, q, θ and Π were determined as described in the text.

Initial concentrations/Σ			Estimated parameters (% S.D.)			
ATP	ADP	AMP	Z	q	θ	Π
0.056	0.913	0.031	3.06 (0.3)	0.918 (0.2)	0.104 (6.1)	2.78 (6.2)
0.318	0.065	0.617	3.25 (1.6)	0.943 (1.5)	0.062 (14.7)	2.61 (0.7)
0.140	0.163	0.697	2.91 (0.2)	0.879 (0.1)	0.147 (4.3)	5.51 (6.3)
0.651	0.062	0.287	3.09 (0.3)	0.950 (0.2)	0.256 (2.6)	0.66 (8.0)
0.060	0.626	0.314	3.26 (0.4)	0.943 (0.3)	0.062 (12.2)	2.61 (13.5)
0.046	0.399	0.555	3.26 (0.2)	0.944 (0.1)	0.081 (6.3)	3.33 (6.0)
			Mean (% S.D.)			
			3.14 (0.5)	0.929 (0.4)	0.119 (7.7)	2.92 (6.8)

and fixation of P_i due to the interconversion of the adenine nucleotides. Some values of the parameters were taken as previously used or determined [1,3]: $\Delta G_p^0 = 8.5$ kcal/mol, $\Delta G_A^0 = 0.15$ kcal/mol and $X_o = 45$ kcal. The other parameters were obtained from the best fit of each experiment as estimated with a nonlinear model fitting routine MODFIT [19] which is based on the Marquardt algorithm [20]. For our calculations we used a straightforward implementation of this program on a PDP 11/40 computer.

For the parameter estimations the original parameters, L terms, of eqs. 15–17 were reexpressed in terms of the more convenient dimensionless parameters degree of coupling $q = L_{po}/\sqrt{L_p L_o}$ and phenomenological stoichiometry $Z = \sqrt{L_p/L_o}$. In addition to the parameter θ introduced in section 3 we chose a new parameter $\Pi = L_A/L_o$ which is a reduced thermodynamic buffer conductance relating the conductance of the adenylate kinase to the conductance of oxidation. By using these definitions we obtain the mapping between the L parameters as defined in eqs. 3–5 and the dimensionless parameters q, Z, θ and Π (see also refs. 1 and 3).

$$L_p = Z^2 L_o \tag{20}$$

$$L_{po} = qZL_o \tag{21}$$

$$L_1 = \theta Z^2 \sqrt{1-q^2}\, L_o \tag{22}$$

$$L_A = \Pi L_o \tag{23}$$

In these expressions L_o appears as a common scaling factor, measuring the amount of mitochondrial protein. This parameter was set to 0.027 to normalize all curves to a common value of L_o which is close to the experimental value determined in previous work [1]. Note that the choice of this parameter is not critical, since it does not explicitly affect the shape of the trajectories. The other parameters q, Z, θ and Π were adjusted by the program MODFIT [19].

Points of the trajectories calculated by numerical integrations of eqs. 15–17 as described in section 3 were sampled at varying time intervals such that adjacent points of a trajectory were about equidistant. A cubic spline function was then used to interpolate between these base points [21]. The minimal distance (Euclidean norm) of each experimental point to the simulated trajectory was determined by using these spline functions. These distances were used to evaluate the residual χ^2 and hence to monitor the search for the best parameter set in the four-dimensional parameter space spanned by the coordinates q, Z, θ and Π. In general, convergence was obtained after about 10 iterations.

The dependence, the correlation matrix and the condition number calculated by the program MODFIT indicated neither overparametrization nor heavy dependence between the four parameters. The maximal dependence was observed between q and Z but was lower than 0.80. All these observations indicate that the chosen model allows a satisfactory fit of the experimental data. This good agreement between the experimental data and the theoretical curves is also apparent from fig. 6.

Table 1 summarizes the results of the parameter estimations of the six individual experiments. These data show that the scatter and the uncertainities of the parameters, indicated by percent standard deviations, were least for the parameters q and Z but larger for θ and Π. Hence, the degree of coupling as well as the phenomenological stoichiometry are fairly constant from one mitochondrial preparation to another. In contrast, the activity of the adenylate kinase, as measured by the parameter Π, shows much larger variations among the different preparations. Since adenylate kinase is localized within the intermembrane space of the mitochondria, it may well be that different amounts of this enzyme leak into the supernatant fraction upon homogenization and resuspension of the mitochondria. Hence, the variations of Π may indicate that this leakage is not well controlled in the standard preparation procedure of the mitochondria. Although no load in the form of an ATP-utilizing reaction has been added to the the incubations, the parameter θ was systematically greater than zero. This indicates the existence of endogenous ATP-utilizing processes in the mitochondrial preparations. As was shown in previous work these processes consist of ATPase [21], Ca^{2+} [22] and H^+ recycling [23] across the inner mitochondrial membrane. Presumably these pro-

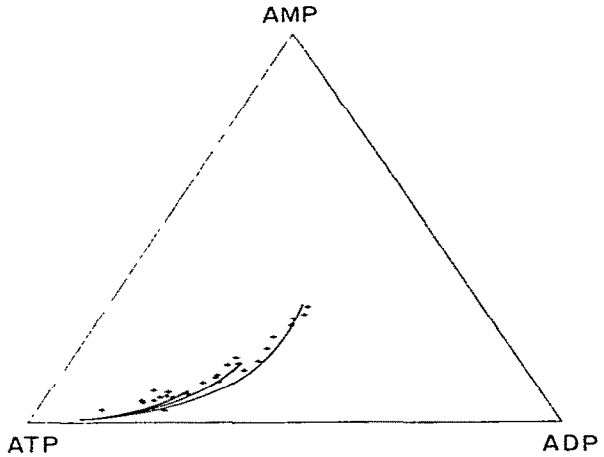

Fig. 7. Experimental verification of the trajectories with different loads. (+) Experimentally determined adenine nucleotide concentrations in mitochondral incubations as described in the text. The solid lines show the theoretical trajectories calculated from eqs. 15–17. The parameters for these integrations were taken from table 2 which contains the best fit values estimated with the routine MODFIT (see text). For the present plot the following mean values from table 2 were used and converted with eqs. 20–23: $Z = 3.04$, $q = 0.93$ (see text), $\Pi = 6.11$. The other fixed parameters were $X_o = 45$ kcal [1], $[P_i] = 8$ mM and $L_{ss} = 0.027$. The values of θ used for the three trajectories are listed in table 2.

cesses depend on the mitochondrial preparations in a much more sensitive and less controllable manner than q and Z. By and large, however, all parameters show that the six individual experiments carried out with differential initial conditions of the adenine nucleotide pool can be simulated by using more or less the same set of parameters. This shows that the values of the parameters are not influenced by the different adenine nucleotide compositions. This underlines once more that the trajectories can be simulated in a satisfactory manner on the basis of eqs. 15–17 within the whole range of the reaction simplex.

A different type of experiment is depicted in fig. 7. Isolated mitochondria were preincubated during 5 min in the presence of 2 mM ATP such that a static head situation was established. Then differing activities of ATPase were injected into the incubation mixture as indicated in table 2.

Table 2

Parameter estimations for experiments with added ATPase

The parameters Z, θ and Π were determined as described in the text. q was held constant at a value of 0.93 (see text and table 1).

ATPase added (IU)	Estimated parameters (% S.D.)		
	Z	θ	Π
0.25	3.02 (0.5)	0.311 (4.2)	10.76 (7.1)
0.5	3.05 (0.3)	0.380 (1.8)	3.05 (10.7)
0.75	3.05 (0.2)	0.479 (1.1)	4.51 (1.5)
	Mean (% S.D.)		
	3.04 (0.3)	–	6.11 (6.4)

Samples were withdrawn and assayed for ATP, ADP and AMP according to the same protocol as given for the previous experiment.

The parameters were estimated again with the help of the program MODFIT with the exception, however, that the value of q had to be fixed. We noted a very poor convergence of the fitting routine when q was allowed to vary, in contrast to the case when this parameter was held constant. Therefore, we have set $q = 0.93$, which is the mean value of the previous experiment, for the estimation of the remaining parameters Z, θ and Π. This appears to be legitimate because also in these experiments Z did not show any large variation. From table 2 it is apparent that an increase in the ATPase activity was paralleled by an increase in θ well above the values of the control experiment in table 1. The adenylate kinase activity as measured by the parameter Π showed a much larger variation than in the controls. The reason for this is unknown but may well be due to a poorer estimation of Π by MODFIT in this type of experiment, especially at the low ATPase activities. Nonetheless, the comparison of the theoretical curves with the experimental data shows that the addition of an ATP-utilizing load in the form of ATPase activity does lead to the predicted changes of the adenine nucleotide concentrations.

In summary, the general kinetic properties of this system can be quite satisfactorily approximated by differential equations based on linear relations between flows and forces with time-con-

stant phenomenological coefficients. It is important to stress that this treatment largely exceeds the domain where these relations are conventionally considered to be valid, namely, the stationary steady state [4,5]. Our experiments and calculations demonstrate therefore that the formulation of nonequilibrium thermodynamics can be extended to describe transient phenomena in a biochemical system.

In the next section we will therefore attempt to approximate the theoretical trajectories by analytical functions such that the numerical integration of the differential eqs. 9–11 can be overcome.

5. Constant of motion and relaxation curves of the adenylate kinase system

In this section we will try to arrive at a deeper understanding of the transient kinetic properties of the system as observed in the foregoing. So far we have noted that, in general, the transient kinetics of the system can be adequately described by a set of equations which are conventionally used in nonequilibrium thermodynamic studies of the steady state. We will now make use of this feature and attempt to approximate the trajectories of the system in terms of purely thermodynamic equations. Bearing in mind that the trajectories are integral curves this is tantamount to attempting an analytical integration of eqs. 9–11, an endeavour which appears to be quite hopeless. However, we can look for judiciously chosen special functions derived from thermodynamic quantities and hope that at least a part of the trajectories coincides with these functions.

To start with, we first consider a quite simple case. In section 3 we noted that at elevated activities of the adenylate kinase the system initially evolved along trajectories corresponding to a constant adenylic energy charge. This suggests that the adenylic energy charge is an integral curve of the adenylate kinase reaction. To be more specific, the adenylic energy charge should be a constant of motion of the system, since at high values of L_A the adenylate kinase flow J_A dominates the other flows J_p and J_I. Hence, we can simplify the scheme in fig. 3 by deleting the arrows representing the influence of J_p and J_I on the adenine nucleotide concentrations. By doing so we then obtain the following simplified set of differential equations:

$$[\dot{A}TP] = L_A X_A \tag{24}$$

$$[\dot{A}DP] = -2L_A X_A \tag{25}$$

$$[\dot{A}MP] = L_A X_A \tag{26}$$

Dividing eq. 25 and eq. 24 yields

$$\frac{[\dot{A}DP]}{[\dot{A}TP]} = -2 \tag{27}$$

Separation of variables allows an integration of eq. 27:

$$\int d[ADP] = -2 \int d[ATP] \tag{28}$$

which is

$$2[ATP] + [ADP] = C \tag{29}$$

We now define a new constant of integration ε by using C and Σ:

$$\varepsilon = \frac{C}{2\Sigma} = \frac{[ATP] + 1/2[ADP]}{[ATP] + [ADP] + [AMP]} \tag{30}$$

which is the well known adenylic energy charge introduced by Atkinson [7]. With this result we are now in the position to state that Atkinson's energy charge assumes the physical interpretation of a constant of motion of the adenylate kinase reaction. If this is the only reaction occurring in the mixture, then the system evolves along a line of constant ε until it reaches the equilibrium line $X_A = 0$. Which line $0 < \epsilon < 1$ is actually chosen depends only on the initial conditions. It is therefore understandable why in cases where J_A dominates all other flows the system must evolve along trajectories which are close to a constant ε.

The other extreme case of the first phase of the trajectories, i.e., the case when L_A and hence the activity of the adenylate kinase is very low, is also simple to explain. Since in this case J_p and J_I dominate the system, the trajectories must evolve along lines characterized by negligible AMP flow. These trajectories are therefore parallel to the baseline of the reaction simplex. As depicted in fig. 4a, the first phase of the trajectories in cases of low values of L_A indeed corresponds to these lines.

We are now left with the problem of finding a simple explanation for the second phase of the trajectories corresponding to the evolution of the system along a common line. Inspection of the results in figs. 2 and 4 suggests that at low activities of the adenylate kinase the system evolves close to lines of a constant phosphate potential whereas at high adenylate kinase activities it evolves close to the equilibrium line $X_A = 0$. This explanation yields, however, no insight into why these lines should behave as relaxation curves of the system.

An understanding of this feature is obtained by calculating the minimal Lyapunov exponent λ_{min} of the system [8,9]. Briefly, a Lyapunov function is a scalar function of the state variables which is positive definite and whose Eulerian derivative is negative definite. A suitable choice of a Lyapunov function of our system is the entropy production which is constrained to be positive definite by the second law [4,5]:

$$\dot{S}T = J_p X_p + J_o X_o + J_A X_A + J_l X_p \geq 0 \tag{31}$$

or

$$\dot{S}T = (L_p + L_l) X_p^2 + 2 L_{po} X_p X_o + L_o X_o^2 + L_A X_A^2 \geq 0 \tag{32}$$

This function is positive except at the state of thermodynamic equilibrium where it is zero. The Eulerian derivative of this function is defined by

$$\ddot{S}T = \frac{\partial \dot{S}}{\partial [ATP]} [\dot{ATP}] + \frac{\partial \dot{S}}{\partial [ADP]} [\dot{ADP}] + \frac{\partial \dot{S}}{\partial [AMP]} [\dot{AMP}] \tag{33}$$

The calculation of this derivative is straightforward and yields the remarkably simple result:

$$\ddot{S}T = -2RT \left[\frac{[\dot{ATP}]^2}{[ATP]} + \frac{[\dot{ADP}]^2}{[ADP]} + \frac{[\dot{AMP}]^2}{[AMP]} \right] \tag{34}$$

Inspection of the right-hand side of eq. 34 shows that the bracket contains only positive terms and therefore we can assert that $\ddot{S}T < 0$. With this we have proven that $\dot{S}$ is indeed a Lyapunov function. This is, by the way, also a sufficient proof for the global asymptotic stability of our system [8,9].

We can now explicitly calculate the Lyapunov exponents of our system defined by

$$\lambda = -\frac{\ddot{S}}{\dot{S}} \tag{35}$$

since the quantities $\dot{S}$ and $\ddot{S}$ are known functions of the thermodynamic forces and the phenomenological coefficients defined by eqs. 6–8, 32 and 34. These Lyapunov exponents permit a piecewise approximation of the temporal evolution of the entropy production $\dot{S}$ throughout the whole reaction simplex through the relation

$$\dot{S}(a,t) = \dot{S}(a_0,t_0)\, e^{-\lambda_{min}(t-t_0)} \tag{36}$$

where a is the concentration vector of the adenine nucleotides defined in section 2. The minimal Lyapunov exponent λ_{min} is defined by

$$\lambda_{min} = \min\left[-\frac{\ddot{S}}{\dot{S}} \right] \tag{37}$$

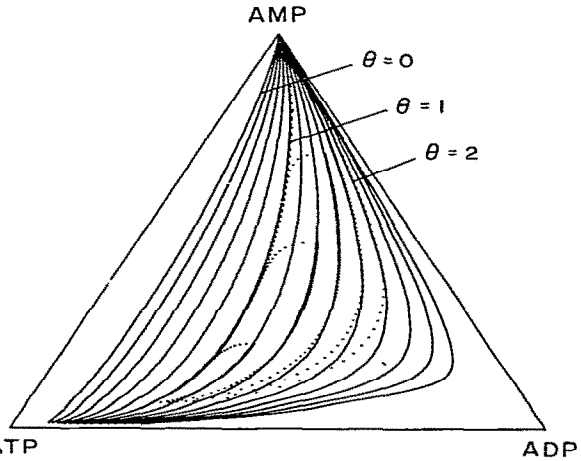

Fig. 8. Relaxation curves. The solid lines depict the loci of minimal Lyapunov exponents λ_{min} for different values of θ. These exponents were searched numerically on the basis of eqs. 32, 34 and 37 along the AMP coordinate by varying AMP from 0 to 1 in increments of 0.01. By joining the adjacent loci of λ_{min} belonging to the same values of θ one obtains the relaxation curves in the reaction simplex. In this figure θ was varied from 0 to 2.6 in steps of 0.2. The other parameters were: $L_p = 0.247$, $L_{po} = 0.0785$, $L_A = 0.2$, $X_o = 50$ and $[P_i] = 8$ mM. The matched load conductance, i.e., for $\theta = 1$, was again $(L_l)_m = 0.0749$. The other values were calculated with the help of eq. 19. Superimposed on these relaxation curves are the dotted trajectories of the load cycles taken from fig. 5b. The relaxation curves are always tangent to these trajectories in the ascending ($\theta > 1$) as well as in the descending ($\theta = 1$) parts. The false impression that the dotted curves may cross the solid lines in this figure is an artifact due to small errors in plotter alignment and plotting. A careful numerical evaluation of these values with extended precision on a digital computer showed that the relaxation curves represent always the extreme limit of the trajectories.

This illustrates that λ_{min} is somehow reminiscent of the minimal eigenvalues of the system and is therefore closely related to the relaxation times which dominate the long-term behavior of the system. Thus, we can imagine that the temporal evolution of the system along the second phase of the trajectory is determined by eq. 37. The trajectories of the system should therefore converge to the loci of λ_{min} for any given set of the L parameters. In other words, the loci λ_{min} in the reaction simplex define the relaxation curve of the system.

In fig. 8 we have plotted the loci of λ_{min} in the reaction simplex for different values of θ. Superimposed in these graphs are the trajectories obtained by numerical integrations of eqs. 15–17 depicted in fig. 5. From this figure it is evident that the second phase of the trajectories indeed converges to the loci of λ_{min}. With this result we have demonstrated that the second phase of the trajectories follows the relaxation curves.

6. Concluding remarks

In this study it has been demonstrated that the transient kinetics of oxidative phosphorylation plus the adenylate kinase can be described on the basis of linear nonequilibrium thermodynamic relations between flows and forces. This result is astonishing for two reasons: (1) The system obeys linearity in a far from equilibrium regime and (2) not only a steady-state situation but also transient behavior obeys linearity. These results appear to be in sharp contradiction to the narrow regime to which linearity is confined on theoretical grounds, i.e., at a steady state in the immediate vicinity of thermodynamic equilibrium [4,6].

In a recent study it was shown that linear relations offer considerable advantages as to the efficiency of biological energy converters [24]. It was speculated that the linearity observed in many biological energy converters operating far from equilibrium is not a consequence of the conventional small force approximation near equilibrium [4,5] but rather a consequence of a feedback regulation maintaining linearity far from equilibrium as a result of evolutionary design [2,24]. This idea is also corroborated by the recent finding that the natural ion transport systems in mitochondria obey linear laws, as long as no artificial ionophores are introduced [25].

Concerning the linearity of the adenylate kinase reaction, we observe that the driving force, the adenylate kinase potential X_A, is of the order of less than 4 kcal for most operating conditions of the mitochondria. Hence, it is also possible that the linearity of this reaction can be simply explained by the existence of a multidimensional inflection point [26] which extends the domain of linearity, especially when the sum of the adenine nucleotides is constant [27]. Needless to say that this linearity, irrespective of its origin, offers, as a byproduct for the investigator, a considerable simplification for the analysis of biological energy conversions.

Furthermore, since linearity allows greater efficiency of energy conversions it is plausible that biological systems make use of this property not only in a steady-state situation but also along a transient between arbitrary steady states within the whole domain of operation of oxidative phosphorylation. This behavior can again be understood as a result of evolutionary design and must therefore not necessarily also apply to chemical reaction mixtures of nonbiological origin.

In our previous studies we have been looking at the adenylate kinase reaction mainly as a thermodynamic buffer system which is chemically and spatially separated from oxidative phosphorylation [2,3]. However, this study has shown that the participation of this reaction in oxidative phosphorylation implies much more. The adenylate kinase reaction acts not only as a thermodynamic buffer, but also regulates the whole transient kinetics of oxidative phosphorylation and sets the operating points of the adenine nucleotides in the cytosol. Therefore, an analysis of the energetics of oxidative phosphorylation cannot be confined to this process alone but should always also consider the effects of the adenylate kinase reaction. This means that oxidative phosphorylation, as a functional unit, not only consists of a redox chain with associated H^+ pumps and the ATPase reaction as stated in every textbook, but also includes the adenylate kinase reaction. This is in line with the common experience that in all aerobic cells with

oxidative phosphorylation invariably also the adenylate kinase reaction is found to be active.

The approximation of the trajectories by the analytical functions in section 5 allows a considerable simplification of the quantitative description of the system by overcoming the need for a numerical integration of the differential equations. In addition, these functions set the limits for the trajectories. Concerning the rapid phase, the limiting trajectory is the line of a constant energy charge as $L_A \rightarrow \infty$. From the simulations shown in fig. 8 and from many other similar numerical calculations not shown here, we conjecture that the relaxation curve acts as an extreme limit for the slow phase of the trajectories, since is no case was it observed that the trajectory was able to cross the relaxation curve.

The next step of the analysis now consists of defining a measure for the thermodynamic buffering power or strength of the adenylate kinase reaction. Preliminary studies have revealed such a measure, a so-called degree of thermodynamic buffering, which is a dimensionless number between 0 and 1 within the whole region of the reaction simplex defined by the limiting analytical functions of section 5. These results will be described in a forthcoming paper.

The analytical functions in section 5 are based on thermodynamic quantities, as is the degree of thermodynamic buffering. Therefore, the whole analysis of thermodynamic buffering, including the transient behavior, can be expressed in terms of nonequilibrium thermodynamic functions only. Needless to say, such a consistent description which considers flows and forces is far superior to an analysis of energy metabolisms carried out in kinetic terms only. Therefore, the choice between a nonequilibrium thermodynamic description of this system and a purely kinetic description is not a matter of 'taste' as has been claimed [28]. Although the kinetic description can say a lot about regulation and control of flows it entirely misses important energetic aspects of energy metabolism such as efficiency, thermodynamic buffering and the like. This has also been realized by the founders of mosaic nonequilibrium thermodynamics [27] or by Hill [29] who therefore combine kinetic and thermodynamic quantities in order to understand the energetics of biochemical reaction systems. In contrast to these approaches, however, which start from a mechanistic reaction scheme with kinetic constants, in our studies we have tried to maintain a purely phenomenological description as far as possible for the sake of generality. Therefore, the results of this study can, in principle, be applied to every other reversible ATP-utilizing system, for example, creatine kinase. Thus, this method of calculating limiting trajectories by deriving the relaxation curves on the basis of minimal Lyapunov exponents offers new insights into the operational features of biological energy converters on a very general level.

Acknowledgements

The authors wish to express their gratitude for stimulating discussions and for fresh ideas to Professors Ora Kedem, Roy Caplan and Gregoire Nicolis. This work was supported by grants from the Swiss National Science Foundation.

References

1 J.W. Stucki, Eur. J. Biochem. 109 (1980) 269.
2 J.W. Stucki, in: Metabolic compartmentation, ed. H. Sies, (Academic Press, London, 1983) p. 39.
3 J.W. Stucki, Eur. J. Biochem. 109 (1980) 257.
4 I. Prigogine, Introduction to thermodynamics of irreversible processes (John Wiley, New York, 1967).
5 A. Katchalsky and P. Curran, Nonequilibrium thermodynamics in biophysics (Harvard University Press, Cambridge, MA, 1965).
6 S.R. de Groot and P. Mazur, Non-equilibrium thermodynamics (North-Holland, Amsterdam, 1962).
7 D.E. Atkinson, Cellular energy metabolism and its regulation (Academic Press, New York, 1977).
8 K. Ogata, Modern control engineering (Prentice Hall, Englewood Cliffs, 1970).
9 J.W. Stucki, Progr. Biophys. Mol. Biol. 33 (1978) 99.
10 H.G. Othmer, in: Modelling of chemical reaction systems, eds. K.H. Ebert, P. Deuflard and W. Jäger (Springer Verlag, Berlin, 1981) p. 2.
11 B.L. Clarke, Adv. Chem. Phys, 43 (1980) 1.
12 G. Hadley, Linear algebra (Addison-Wesley, Reading, MA, 1973).
13 P.B. Garland, Biochem. Soc. Symp. 27 (1968) 41.
14 D. Johnson and H.A. Lardy, Methods Enzymol. 10 (1967) 94.

15 S.N. Graven, H.A. Lardy and A. Rutter, Biochemistry 5 (1966) 1735.
16 P.E. Linnett, A.D. Mitchell, M.D. Partis and R.B. Beechy, Methods Enzymol. 55 (1979) 337.
17 W. Lamprecht and I. Trautschold, in: Methoden der enzymatischen analyse, ed. H.U. Bergmeyer (Verlag Chemie, Weinheim/Bergstr., 1970) p. 2024.
18 D. Jaworek, W. Gruber and H.U. Bergmeyer, in: Methoden der enzymatischen analyse, ed. H.U. Bergmeyer (Verlag Chemie, Weinheim/Bergstr., 1970) p. 2051.
19 J.E.A. McIntosh and R.P. McIntosh, Mathematical modelling and computers in endocrinology (Springer Verlag, Berlin, 1980).
20 P.R. Bevington, Data reduction and error analysis for the physical sciences (McGraw-Hill, New York, 1969).
21 J.W. Stucki and P. Walter, Eur. J. Biochem. 30 (1972) 60.
22 J.W. Stucki and E. Ineichen, Eur. J. Biochem. 48 (1974) 365.
23 J.W. Stucki, Eur. J. Biochem. 68 (1976) 551.
24 J.W. Stucki, M. Compiani and S.R. Caplan, Biophys. Chem. 18 (1983) 101.
25 D. Pietrobon, M. Zoratti, G.F. Azzone, J.W. Stucki and D. Walz, Eur. J. Biochem. 127 (1982) 483.
26 K.J. Rothschild, S.A. Ellias, A. Essig and H.E. Stanley, Biophys. J. 30 (1980) 209.
27 H.V. Westerhoff, Mosaic non-equilibrium thermodynamics and the control of biological free-energy transduction, Doctoral Thesis, University of Amsterdam, Drukkerij Gerja, Waarland (1983).
28 J.G. Reich and E.E. Sel'kov, Energy metabolism of the cell (Academic Press, London, 1981).
29 T.L. Hill, Free energy transduction in biology (Academic Press, New York, 1977).